Metal/semiconductor phase transition in chromium nitride(001) grown by rf-plasma-assisted molecular-beam epitaxy

Costel Constantin, Muhammad B. Haider, David Ingram, and Arthur R. Smith[a)]
Condensed Matter and Surface Science Program, Department of Physics and Astronomy, Ohio University, Athens, Ohio 45701

(Received 15 June 2004; accepted 20 October 2004)

Structural and electronic properties of stoichiometric single-phase CrN(001) thin films grown on MgO(001) substrates by radio-frequency N plasma-assisted molecular-beam epitaxy, are investigated. *In situ* room-temperature scanning tunneling microscopy clearly shows the 1×1 atomic periodicity of the crystal structure as well as long-range topographic distortions which are characteristic of a semiconductor surface. This semiconductor behavior is consistent with *ex situ* resistivity measurements over the range 285 K and higher, whereas below 260 K, metallic behavior is observed. The resistivity-derived band gap for the high-temperature region, 71 meV, is consistent with the tunneling spectroscopy results. The observed electronic (semiconductor/metal) transition temperature coincides with the temperature of the known coincident magnetic (para-antiferro) and structural (cubic-orthorhombic) phase transitions. © *2004 American Institute of Physics*.
[DOI: 10.1063/1.1836878]

For many years, CrN has received a lot of attention due to its high hardness and corrosion resistance.[1,2] In addition, CrN is also interesting due to its magnetic, optical, and electronic properties. It is known that CrN is paramagnetic (PM) with a B1 NaCl crystal structure at room temperature; at $T_{\mathrm{Néel}}$, reported in the range of 273–283 K, the material undergoes a phase transition to antiferromagnetic (aFM) with an orthorhombic P_{nma} crystal structure.[3–5] Filippetti *et al.*[6] found theoretically that the magnetic stress is the driving force for the lattice distortions, and thus linked the magnetic and structural transitions. So far, however, the electronic properties have been less understood.

Filippetti *et al.*[5] reported, based on theoretical calculations, that CrN is a metal in its PM state but a weak metal in the aFM state. This agrees well with an earlier experimental work, based on CrN polycrystalline powders, which found metallic behavior with, however, an abrupt increase of the resistivity with increasing temperature at ~286 K.[7] On the other hand, Herle *et al.*,[8] based on synthesized CrN powders, reported that CrN is a semiconductor with a band gap of 90 meV as measured by resistivity. Recently, Gall *et al.*[9] grew crystalline thin films of CrN by sputtering and reported that CrN behaves as a semiconductor (Mott-type insulator) with an optical gap of 0.7 eV. Although the electronic behavior at room temperature has become more clear, the value of the band gap as well as its detailed nature, remain to be determined; moreover, the discrepant results reported for low temperatures, remain to be resolved.

In this letter, we present results concerning the unique structural and electronic properties of CrN(001). We show that high-quality epitaxial layers are grown by molecular-beam epitaxy (MBE), having crystalline (001) orientation and atomically smooth surface [as measured by scanning tunneling microscopy (STM)] and semiconducting behavior at 300 K. Bulk *ex situ* measurements confirm the semiconducting behavior at 300 K, but furthermore a transition to the metallic state is observed at ~285 K. This transition coincides with the known magnetic/structural transition.

The experiments are performed in a custom-designed hybrid MBE/STM system. The MBE system employs a Cr effusion cell and a radio-frequency N plasma source with N_2 as the source gas. During the entire growth, the N plasma source is set to a power of 500 W with the nitrogen flow rate about 1.1 sccm (growth chamber pressure is 1.1×10^{-5} Torr). The entire growth process is monitored by reflection high energy electron diffraction (RHEED), after which the samples are transferred to the *in situ* STM. Finally, x-ray diffraction (XRD) and resistivity versus temperature (*R*–*T*) measurements are performed *ex situ*. Resistivity is measured using the four-point van der Pauw geometry.

The MgO(001) substrates are first heated to 900 °C for 30 min under the presence of N plasma, after which the RHEED pattern looks streaky [Fig. 1(a)], indicating a suitable smooth substrate surface. A buffer layer of CrN is grown at a sample temperature $T_s<200$ °C with thickness $t_B\sim45$ nm. The RHEED pattern of the buffer layer [Fig. 1(b)] looks spotlike, suggesting rough growth. Next, the temperature is increased to ~450 °C and a CrN layer is grown with a thickness of $t_{\mathrm{CrN}}\sim90$ nm, after which the RHEED pattern [Fig. 1(c)] shows a streaky behavior but also some extra spots. At this point, the Cr shutter is closed, followed by a second and rapid increase of T_s to 650 °C. The RHEED pattern becomes more streaky [Fig. 1(d)] and the extra spots fade away. After ~14 min at 650 °C, a final ~4 nm CrN layer is grown. The ultimate RHEED pattern [Fig. 1(e)] is very streaky suggesting a high-quality atomically smooth surface with (001) orientation.

Shown in Fig. 2 are the main peaks seen in XRD over the range $30°<2\theta<140°$ — the two orders (002 and 004) of MgO and CrN. The Cu $K\alpha_1$ and $K\alpha_2$ 002 peaks of MgO (CrN) are seen at $2\theta=42.99°$ and 43.10° ($2\theta=43.92°$ and 44.02°), respectively. The inset of Fig. 2 shows the Lorentzian fit for the rocking curve of the CrN 002 peak, giving a full width half maximum (FWHM) of the $K\alpha_1$ CrN 002 peak of $\Gamma_\omega=0.09°$, which is smaller than the corresponding Γ_ω

[a)]Author to whom correspondence should be addressed; electronic mail: smitha2@ohio.edu

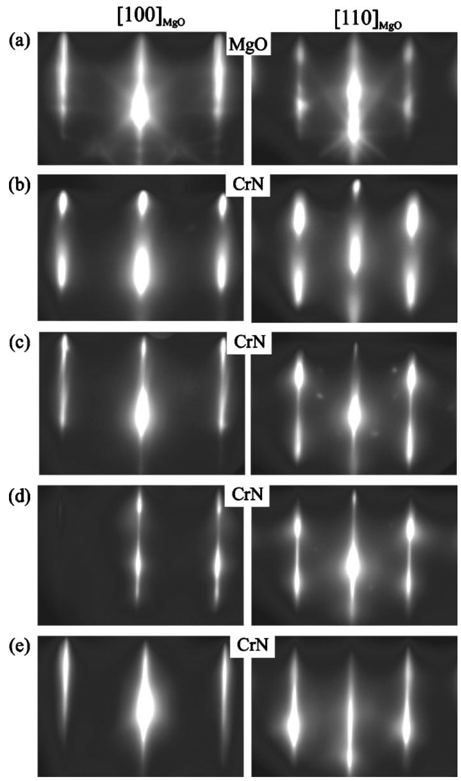

FIG. 1. Sequence of RHEED patterns during the CrN growth on MgO(001) substrate. (a) MgO substrate after the heating; (b) CrN buffer layer; (c) CrN layer grown at 450 °C; (d) After the temperature of the substrate goes up to 650 °C with the plasma on for about 10 min; and (e) the final layer of CrN.

=0.10° of the MgO 002 substrate peak. This further indicates the high-quality crystallinity of the CrN film.

Lattice parameters measured for several CrN(001) films are summarized in Table I. The measured *out-of-plane* lattice constant $a_\perp \simeq 4.14$ Å is consistent with values of 4.14–4.18 Å reported in earlier work.[7,10] The measured *in-plane* lattice constant $a_\parallel$ obtained from RHEED varies from 4.04 Å for the thinnest film ($t_{CrN}=335$ Å) to 4.13 Å for the thickest film ($t_{CrN}=1490$ Å), increasing with thickness. The thinnest films are evidently *in-plane* compressively strained. Note that $a_\perp \simeq a_\parallel$ for thicker films and that the agreement between $a_\perp$ and $a_\parallel$ improves with thickness. Moreover, the relaxed lattice constant a_0 is obtained for each film using the following equation with ν being the Poisson ratio for CrN.[9,1]

$$a_0 = a_\perp \frac{1-\nu}{1+\nu} + a_\parallel \frac{2\nu}{1+\nu}. \qquad (1)$$

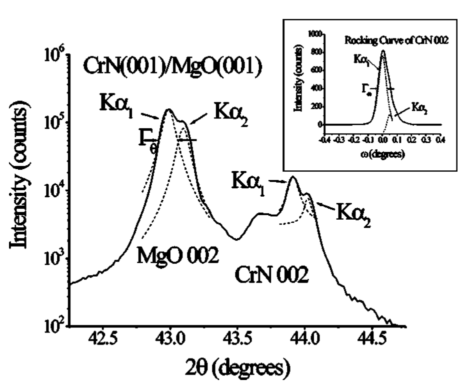

FIG. 2. XRD results for CrN(001)/MgO(001). Lorentzian fittings of $K\alpha_1$ and $K\alpha_2$ of MgO 002 and CrN 002 peaks; (inset) rocking curve of CrN 002 peak.

TABLE I. CrN 002 FWHM, lattice constants $a_\perp$, $a_\parallel$, and a_0, for three different film thicknesses of CrN(001)/MgO(001).

CrN sample	250	262	256
Thickness of CrN layer t_{CrN}(Å)	335	894	1490
CrN 002 FWHM $F\omega$(°)	0.13	0.09	0.12
Lattice constant $a_\perp$(Å)	4.14	4.13	4.14
Lattice constant $a_\parallel$(Å)	4.04	4.06	4.13
Relaxed bulk lattice constant a_0(Å)	4.10	4.10	4.14

With $\nu=0.29$, the relaxed lattice constant a_0 obtained is 4.10 Å for the two thinnest (<1000 Å) films but for the thickest film $a_0=4.14$ Å—which we conclude to be the most probable relaxed bulk value for CrN and consistent with previously reported values of 4.13–4.185 Å.[9,11,12]

Regarding the stoichiometry, Rutherford backscattering has been done for our thickest film ($t_{CrN}=1490$ Å) and it was found that Cr:N=1:1 with ~5% uncertainty.

Figure 3 shows room-temperature STM images of CrN(001) acquired at sample bias $V_s=+0.7$ V. The surface of CrN, on a scale of 300 Å×300 Å [Fig. 3(a)], consists of smooth terraces seprated by steps of height 2.07 Å ($a_0/2$) which indicates that the growth is epitaxial. The atomic resolution image of CrN(001) in Fig. 3(b) clearly shows the cubic 1×1 structure. The atoms viewed in this image are most likely Cr, although a detailed surface calculation remain to be performed. The conventional surface cell , and the primitive surface unit cell rotated by 45° are shown. Features 1 and 2 in Fig. 3(b) are most likely CrN vacancy islands which formed during heating up to 650 °C. In the image of Fig. 3(c), besides CrN vacancy islands (3, 4, and 5), there are some brighter areas labeled A, B, and C. Similar features, referred to as long-range-topographic distortions (LTDs),[14] have been observed recently by Al-Brithen *et al.*[13] on the

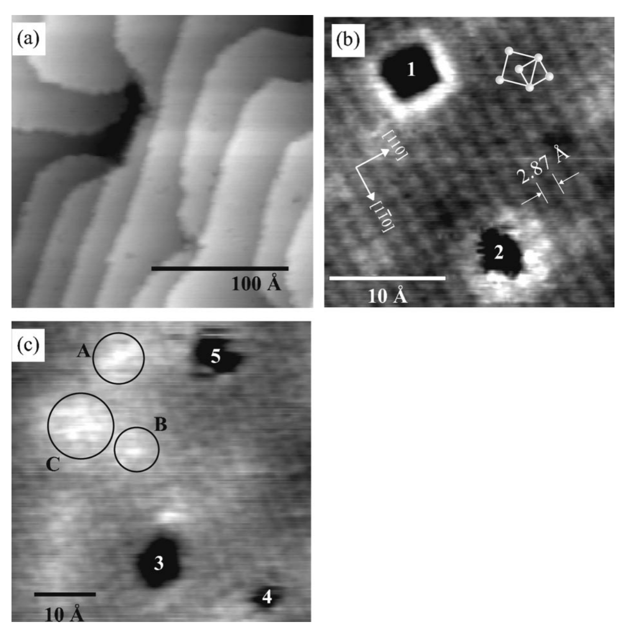

FIG. 3. Room-temperature STM of CrN(001)/MgO(001). (a) 250 Å×250 Å STM image of CrN showing smooth terraces. $V_S=+1V$, $I_T=0.2$ nA; (b) 25 Å×25 Å atomic resolution image showing the 1×1 square lattice periodicity and the face-centered-cubic conventional unit cell of the CrN lattice. $V_S=+0.7$ V, $I_T=0.2$ nA; (c) The features at A, B, and C are LTDs. The features 1–5 are CrN vacancy islands. $V_S=+0.6$ V, $I_T=0.6$ nA.

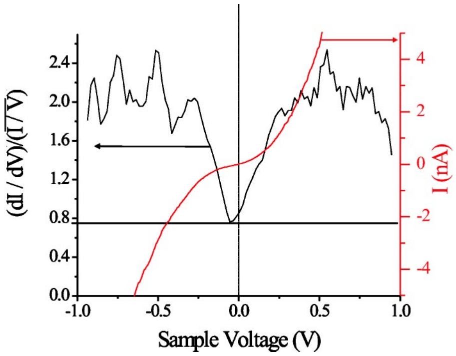

FIG. 4. STS of CrN(001)/MgO(001). I–V_S curve (right axis) taken on similar image area as in Fig. 3(c); together with NC-V_S (left axis) derived from I–V_S curve.

nonpolar (001) surface of semiconducting ScN as well as for various nonpolar (110) surfaces of III–V semiconductors like GaAs.[14] They are only observed on semiconductor surfaces. For example, they are not seen on MnN(001) or $Mn_3N_2(010)$ surfaces in our system, which are metallic.[15] The explanation of the mechanism of the LTD features has been explained elsewhere,[14,16] but briefly (for this case) the LTDs can be attributed to downward band bending in the vicinity of positively charged ionized donors, which locally enhances the tunneling current (for either bias polarity).

Room-temperature scanning tunneling spectroscopy (STS) measurements averaged over an area as in Fig. 3(c) have been performed. The current–voltage $(I–V_S)$ curve is presented in Fig. 4 (right axis), showing a nonlinear shape, typical of a semiconductor. The corresponding normalized conductance $(\mathrm{NC}) \equiv (dI/dV)/(\overline{I/V})$, which is related to the local density of states (LDOS), is plotted versus V_S in Fig. 4 (left axis) and was computed according to the method described by Feenstra,[17] using a broadening of 0.05 V. The NC-V_S spectrum shows that a dip in the LDOS is observed near the Fermi level (the zero of the voltage in Fig. 4). Such a dip is consistent with a small band gap; however, the 300 K thermal broadening ($\sim$50 meV) precludes a direct measure of its size. Qualitatively, the Fermi level E_F is on the conduction-band side of the minimum, implying the sample is *n* type, which agrees with a separate hot-point probe measurement, which showed that the majority carriers are electrons.

To confirm the semiconductor behavior seen in STM at 300 K, *ex situ* resistivity versus temperature $(\rho–T)$ measurements were taken between 77 and 450 K. As shown in Fig. 5, the resistivity varies linearly (slightly increasing) with increasing T between 77 and 260 K [Region (I)], showing metallic behavior. At 260 K, ρ begins to increase more, and above 280 K, ρ increases steeply, consistent with a first-order phase transition. Above 280 K [Region (II)], ρ decreases exponentially with temperature, indicating semiconductor behavior. Measuring $\rho–T$ with decreasing temperature, thermal hysteresis is observed with a width of 20 K. As mentioned before, a steep increase in ρ has been observed by Tsuchiya *et al.*[18] and Browne *et al.*[7] but not a transition from metallic to the semiconductor state, as we observe.

Plotted as an inset of Fig. 5 is $\ln(\rho/\rho_0)$ versus $1/T$ for the data of Region (II). Fitting the data using the linear equation $\ln(\rho/\rho_0)=(E_g/2k_B)(1/T)$, we derive the band gap $E_g=71.0\pm0.3$ meV with $\rho_0=4.52\times10^{-3}\ \Omega$ cm.

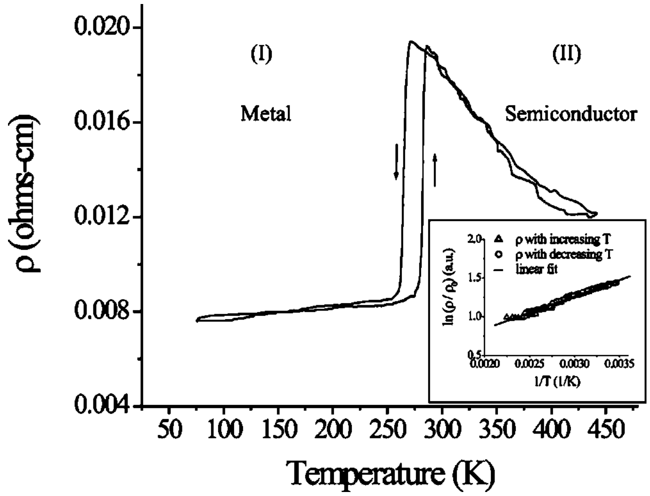

FIG. 5. ρ vs T measurement showing metallic (I) and semiconductor (II) regions. There is evident thermal hysteresis with a width of $\sim$20 K. The inset shows the linear fit of ln (ρ/ρ_0) vs $1/T$ region (II), the straight line represents the linear fit to the data having slope$=(E_g/2k_B)$.

In summary, it has been shown that high-quality epitaxial CrN(001) layers on MgO(001) substrate have been prepared by MBE. *In situ* STM data acquired at 300 K shows semiconductor behavior which agrees well with *ex situ* $\rho–T$ measurements, above the transition, but below the transition metallic behavior is obtained. This transition occurs at the same temperature range as the well-known magnetic and structural transition, which suggests that all three transitions may be correlated.

This work was supported by the National Science Foundation under Grant Nos. 9983816 and 0304314. The authors acknowledge useful discussions with H. Al-Brithen, and H. H. Richardson.

[1]U. Wiklund, M. Bromark, M. Larsson, P. Hedenqvist, and S. Hogmark, Surf. Coat. Technol. **91**, 57 (1997).
[2]C. Nouveau, M. A. Djouadi, O. Banakh, R. Sanjinés, and F. Lévy, Thin Solid Films **398**, 490 (2001).
[3]L. M. Corliss, N. Elliott, and J. M. Hastings, Phys. Rev. **117**, 929 (1960).
[4]M. N. Eddine, F. Sayetat, and E. F. Bertaut, C. R. Seances Acad. Sci., Ser. B **269**, 574 (1969).
[5]A. Filippetti, W. E. Picket, and B. M. Klein, Phys. Rev. B **59**, 7043 (1999).
[6]A. Filippetti and N. A. Hill, Phys. Rev. Lett. **85**, 5166 (2000).
[7]J. D. Browne, P. R. Liddell, R. Street, and T. Millis, Phys. Status Solidi **1**, 715 (1970).
[8]P. S. Herle, M. S. Hedge, N. Y. Vasathacharya, S. Philip, M. V. R. Rao, and T. Sripathi, J. Solid State Chem. **134**, 120 (1997).
[9]D. Gall, C. S. Shin, R. T. Spila, M. Odén, M. J. H. Senna, J. E. Greene, and I. Petrov, J. Appl. Phys. **91**, 3589 (2002).
[10]D. Gall, C. S. Shin, R. T. Haasch, I. Petrov, and J. E. Greene, J. Appl. Phys. **91**, 5882 (2002).
[11]P. Hones, M. Diserens, R. Sanjines, and F. Levy, J. Vac. Sci. Technol. B **18**, 2851 (2000).
[12]P. M. Fabis, R. A. Cooke, and S. McDonough, J. Vac. Sci. Technol. A **8**, 3819 (1990).
[13]H. A. Al-Brithen and A. R. Smith, Phys. Rev. B **70**, 045303 (2004).
[14]K. -J. Chao, A. R. Smith, and C. K. Shih, Phys. Rev. B **53**, 6935 (1996).
[15]H. Yang, H. Al-Brithen, A. R. Smith, J. A. Borchers, R. L. Cappelletti, and M. D. Vaudin, Appl. Phys. Lett. **78**, 3860 (2001).
[16]J. A. Stroscio, R. M. Feenstra, and A. P. Fein, Phys. Rev. Lett. **58**, 1668 (1987).
[17]R. M. Feenstra, Phys. Rev. B **50**, 4561 (1994).
[18]Y. Tsuchiya, K. Kosuge, Y. Ikeda, T. Shigematsu, S. Yamaguchi, and N. Nakayama, Mater. Trans., JIM **37**, 121 (1996).